1 2 3 4 5 6

Use of Data Assimilation for Inference of CA1 Neuron Pathology in 3xTg Mouse Model of Alzheimers

Daniel Breen[1], Clark A. Briggs[5], Grace E. Stutzmann[6], Henry D.I. Abarbanel[2,3,4]

February 28, 2017

Abstract

Experiments used to characterize altered electrical and molecular properties of neurons in Aβ are laborious and may fail to detect variability and multifaceted differences in and across populations of neurons. We present techniques of data assimilation together with a data mining approach to investigate pathology in the 3xTg mouse model of Alzheimer's disease combining both amyloidopathy and tauopathy. We find differences in individual intrinsic excitability and use our biophysically tuned models to propose mechanisms underlying these differences. The scientific contribution is primarily methodological, as we presently wish only to show a proof of principle of the methods. We set a foundation to extend the methods towards investigating alterations in Ca^{2+} dynamics and medical applications.

1 Introduction

While the etiology of Alzheimer's disease (AD) is unknown, the production of beta-amyloid peptides (Aβ) [13] and disruption of Ca^{2+} signaling [21, 36] in the brain are involved. Histopathological features of AD, including amyloid and tau pathology, interact with the calcium signaling dysregulations in a vicious spiral [39, 37].

*[1]Department of Physics, University of California - San Diego, CA, USA.

†[2] Distinguished Professor, Department of Physics, University of California - San Diego, CA, USA.

‡[3] Marine Physical Laboratory (Scripps Institution of Oceanography), University of California - San Diego, CA, USA.

§[4] Center for Engineered Natural Intelligence, University of California - San Diego, CA, USA.

¶[5] Department of Neuroscience, Rosalind Franklin University of Medicine and Science, The Chicago Medical School, North Chicago, IL 60064, USA

‖[6] Professor, Department of Neuroscience, Rosalind Franklin University of Medicine and Science, The Chicago Medical School, North Chicago, IL 60064, USA

What is now lacking in the understanding of neuropathology are the links between underlying causes at the molecular, single cell, and circuits level of the disease and the behavioral symptoms. Computational modeling offers the potential to link across the different levels of genes and drugs, synapses and neurons, and cognition and behavior to provide a unified, testable basis for formulating therapeutic strategies [11, 10, 4, 24, 26, 49].

Mathematical models have been applied to the study of Aβ related excitability changes [10, 26, 49]. Biophysical neuron models such as conductance based Hodgkin Huxley (HH) type models contain interpretable and biologically meaningful parameters capable of reproducing experimentally observed membrane dynamics. Such models thus provide a framework in which to identify changes in biophysical properties of diseased cells in a manner that elicits targets for potential therapeutic intervention.

Neurophysiological studies often focus on how AD pathology disturbs synaptic function [6, 8, 18, 32, 33, 34, 48]. More recently, alterations in intrinsic neuronal properties have been examined [4, 12, 23, 5, 10, 40, 41, 14, 17, 45, 31]

We wish to identify quantitative changes in the detailed electrical membrane dynamics between wild type and diseased cells where the latter have been genetically modified, in mice, to produce analogs to human Alzheimer's responses. These 3xTg-AD mice express mutant presenilin (PS1), Aβ precursor protein (APP), and tau, and develop both plaques and tangles in an age and region dependent manner [27, 28]. The goal is to further develop HH like models of cortical cells implicated in Alzheimer's disease and to inform the use of well designed experiments which will quantify changes, including intracellular Ca^{2+} dynamics of these cells. Models will incorporate enough biological realism to be useful tools in the neuropharmacological process of drug design, such as by prescreening a number of compounds for bench testing in the laboratory. An example would include using the estimated models as a readout for alterations in Ca^{2+} dynamics and molecular signaling pathways, an area that has been identified as a target mechanism where the initial stages of Alzheimer's can be tracked and where further degeneration of 3xTg cellular behavior can be potentially identified and treated [7]. The present work investigates alterations in neuronal intrinsic excitability, and sets foundations which can be used to attend to alterations of Ca^{2+} dynamics in future work.

We have previously developed methods of statistical data assimilation which have been successful in incorporating information in complex chaotic and neural systems, from incomplete data sets [43, 20, 1, 19, 22, 47, 46, 15, 25].

Other methods of parameter fitting in neuron systems include hand-tuning [35], parameter space exploration [3, 29, 30], gradient descent [3], and evolutionary algorithms [42, 16, 2]. These methods have yielded the estimation of many states and parameters as well, but with one or more of the following limitations [9]:

- parameter identifiability issues are not addressed
- the parameters must be heavily constrained, reflecting unlikely prior knowledge

- only parameters which enter the model linearly can be accurately estimated
- make adequate "best fits" but fail to predict

The first and last are crucial shortcomings - work in single neuron modeling often does not raise the issue about the uniqueness of estimated parameters [9], nor does it often consider the subjectivity of a good fit. Hand tuning is highly subjective, and even if a 'good' parameter set can be found, it is never certain if there is a better one that has not been discovered. Methods incorporating a heuristic metric of error, including parameter space exploration and evolutionary algorithms, may miss best parameter sets and have poor predictive power.

The approach advanced here directly addresses the issue of testable model fitting in neural systems. Previously [43, 20, 19, 22, 15, 25], it has demonstrated success in estimating all of the parameters in HH conductance models, including those that enter nonlinearly such as the gating kinetics describing the ion currents. They have also been shown capable of predicting precise waveform information of the voltage of a neuron evolving in time according to a novel stimulating current.

2 Methods

2.1 CA1 Neuron Model

One of the limitations of minimizing a smooth loss function is the danger of getting stuck in local minima. This tends to yield a number of different parameter sets which produce fit the data well and have good predictive power. A more complex model including more ionic currents would have the advantage of incorporating some elements of biological realism. However, we are interested in finding alterations in parameters and features which can be used to distinguish populations of neurons in a biophysical context, so we must take into consideration this parameter identification problem.

We subjected different neuron models, some including Ca^{2+} dynamics, to our methods of parameter estimation. Although we wish to identify alterations in Ca^{2+} dynamics in 3xTg cells, these models encountered substantial parameter identifiability obstacles that remain to be overcome. Instead, we settled with a basic HH model, as it is a biophysically realistic model which provides a simplified arena in which to cope with obstacles of parameter identifiability. The basic HH model did better at reproducing many features of the data without the parameter identification issues of more complicated models. This will set a foundation for future refinements including calcium and calcium activated potassium currents in the model, which are able to address investigating alterations in calcium dynamics.

In our experiments collecting voltage data, we use a current clamp setup, where voltage traces are measured with a known injected current. Intuitively, one example of parameter unidentifiability is that different depolarizing and

repolarizing currents can contribute to the opening and closing of ion channels underlying voltage response to injected current. Using only measured voltage, it is difficult to determine what the relative contributions of different ionic currents are to characteristics of features of the voltage waveform.

Our CA1 neuron model is thus a basic Hodgkin-Huxley (HH) neuron with only sodium (I_{Na}), potassium (I_K), and leak (I_L) currents:

$$\begin{aligned} C_m \frac{dV(t)}{dt} &= g_{Na} m(t)^3 h(t)(E_{Na} - V(t)) + g_K n(t)^4 (E_K - V(t)) \qquad (1) \\ &\quad + g_L(E_L - V(t)) + I_{injected}(t) \\ \frac{dx(t)}{dt} &= \frac{x_\infty(V) - x(t)}{\tau_x(V)} \\ x_\infty(V) &= 0.5(1 + \tanh(\frac{V - \theta_x}{\sigma_x})) \\ \tau_x(V) &= t_{x0} + t_{x1}(1 - \tanh^2(\frac{V - \theta_x}{\sigma_{xt}})) \qquad (2) \end{aligned}$$

Here $V(t)$ is the membrane voltage, C_m is the membrane capacitance, and $I_{injected}(t)$ is a known stimulating current injected into the neuron in a current clamp setup. g_i and E_i denote the maximum conductance and reversal potential for current i, respectively.

The equations for x are a shorthand for the kinetics of the gating variables m, h, and n. $x_\infty(V)$ is the voltage dependent steady state activation which depends on θ_x, the voltage at half activation, and σ_x, the width of this activation. $\tau_x(V)$ is the voltage dependent relaxation time, describing the rate that the gating variables change to their steady state values.

Errors in the descriptions of the dynamics of these channels in HH models and noisy measurements contribute to the parameter identifiability problem. We show, using our data assimilation algorithm described in section 2.2, that we can find sets of parameters in a basic HH model capable of reproducing nearly exactly the shape of the waveform of our recorded data. Correctly predicted features include the shape of the action potential waveform, afterhyperpolarization effects, refractory periods, spike timing, and subthreshold variations. Examples of predictions are displayed in Figure 1.

Our strategy here is to estimate ensembles of models and look for similarities and differences in patterns in these ensembles across distinct populations of neurons. Since there are many sets of model parameters which are compatible with the observed data, we do not attempt to pinpoint a unique 'correct set' of model parameters. Each set of model parameters possessing good predictive power is assumed to be as good as any other set. We do retain some element of subjectivity in that estimated models are said to be compatible with the data when predictions, generated by integrating the model beyond the estimation, are judged to match the subthreshold voltage variations and spike timing. This subjective evaluation was generally easy as matches to the data were either very good or very poor.

This validation procedure is easily scalable as the process was automated by checking the value of a number of features at the end of the data assimilation procedure, including the use of a spike sorting algorithm which checked whether the prediction contained action potentials with a duration within a biologically realistic range (no more than several ms) and whether the value of the objective function, defined in section 2.2, was smaller than a cutoff value. The cutoff value was easily determined as the objective function tended to take either large or small values which corresponded to very poor or very good fits, respectively.

2.2 Methods of Data Assimilation

Data assimilation refers to analytical and numerical procedures in which measurements and models are combined to infer knowledge about a system which is not available in the measurements alone. Information in measurements is transferred to model dynamical equations selected to describe the processes thought to produce the data. The problem is typically formulated as follows. We formulate a model describing the system with state variables $\mathbf{x}$ defined at times $t_0, t_1, ..., t_T$, and we seek to infer the model state variables at the end of the estimation window $\mathbf{x}(t_T)$ and the unknown model parameters $\mathbf{p}$.

One of the difficulties commonly encountered in data assimilation arises from the fact that systems in the real world almost always contain processes that the modeler is ignorant about or cannot represent. Another difficulty comes from the fact that measurements are noisy, which limits the ability to infer properties of systems even in the presence of perfect models. Estimating properties of the dynamics of systems which are nonlinear, such as neurons, only compounds these problems. Previously, we have developed methods of data assimilation capable of dealing with gaussian measurement noise when the neural system under study is perfectly described by a basic HH model [43, 20, 19, 15]. As our focus here is on data from real neurons, we cannot hope to have a perfect model, but past studies provide a firm basis on which to build our understanding here.

We have applied a variational approach which has been used successfully for estimating models of neurons, using data from neurons in region hvc of the avian song system, in [22, 25] and remains a reliable choice in complex or simpler models, including our basic HH model of CA1 neurons here. A critical concern in variational approaches to nonlinear dynamical systems is that the familiar least-squares objective function may give an irregular search surface with many local minima. We addressed this problem here by including a balanced synchronization term, $u(t)(V_{data}(t) - V(t))$, in the model dynamics, which regularizes and minimizes the influence of local minima by ensuring that the solution set defines a model that is capable of synchronizing with the data. The objective function includes a penalty for this regularization and is taken as

$$\sum_{t=1}^{T} (V_{data}(t) - V(t))^2 + u(t)^2 \tag{3}$$

where $V_{data}(t)$ is the measured voltage, $V(t)$ is the voltage output from the

model, and T is the number of discretely sampled time points in the estimation window. $u(t)$ describes the magnitude of the synchronization term.

The neuron model that we investigated is not known to be chaotic for the biophysical range of our parameters, but it is nonlinear, and in the high-dimensional search space, there may well exist chaotic regions that must be explored by the optimization routine, and these will benefit from this regularization. If a solution to the model can be found that is consistent with the data, the value for the control parameter $u(t)$ should become small relative to the model dynamics at the end of the optimization. The quality of the model was tested by setting $u(t)$ to zero and integrating the model forward from the end of the assimilation period using the estimated parameter and state values.

The implementation of the data assimilation algorithm was accomplished through the use of the open source software package IPOPT (Interior Point OPTimizer) with the linear solver ma57 [44].

2.3 Detecting Altered Features and Mechanisms

We are interested in identifying features of membrane electrical behavior in our neuron models which are different between two strains, 3xTg and nonTg. Using the estimated models, the number of features was expanded from the set of 20 estimated parameters in the models to include approximately 100 total features.

The predictions, obtained by integrating the model forward past the end of the estimation window, are the red traces such as those shown in Figure 1.

We trained random and regression forest models using the features and model parameters to predict labels of interest, including the known type of each neuron (3xTg or nonTg), threshold voltage, spike half-width, and other features. We used the feature importance attribute of the trained models to determine the relative importance of each feature in predicting the value of each label.

We also calculated kernel density functions over the data points in three dimensional subspaces of the 100 dimensional feature space. We used these density functions to estimate the overlap of three dimensional probability distributions describing the 3xTg and nonTg neurons. Feature importances significantly reduce the number of feature subspaces to examine when searching for differences between the two populations.

We have used regression forests to detect predictors of altered features between 3xTg and nonTg strains. These can include model parameters and other features. An example includes discovering other features and model properties predicting intrinsic excitability. Threshold voltage and the rheobase are examples of features quantifying intrinsic excitability. By finding predictors of quantities such as these, we are able to propose mechanisms causing the observed differences in the two populations of neurons. We also computed correlations among these model parameters and features, though in some cases relationships are nonlinear.

It may be that features detected to be altered differ only between subsets of 3xTg and nonTg. In this case, if two features A and B are found to be altered, it may be that A is altered in some neurons while B is unaltered in a other

neurons. Then, in some neurons, feature B may be altered, while A is unaltered in others. A decision tree may reveal this kind of structure, while a table of variable importances will not. For clarity and simplicity of the presentation, we do not include decision trees, but mention in passing that splits along different features descending down the decision tree supported this notion.

In our set of recordings, an epoch is defined as each instance in which recordings are obtained from a neuron by eliciting a response with a stimulating current. Each epoch usually involves the neuron being stimulated with a new injected current.

Using our methods of data assimilation, we estimated model parameters for 56 epochs from 5 3xTg and 6 nonTg neurons. For each data set, we initialized our data assimilation search procedure with 500 distinct sets of parameters sampling each parameter from a uniform distribution defined between the parameter bounds. At the end of search procedure, many of these parameter value initializations did not result in an estimated model which passed the validation tests described in section 2.1. These were not included in the processed data set used to draw inferences about differences between 3xTg and nonTg neuron populations.

In order to balance out the contribution from each neuron and class in the data, we sampled with replacement from the pool of estimated parameter sets so that each neuron contributed an equal number of samples to its respective class. Finally, we ensured that the 3xTg and nonTg pools had equal size.

3 Results

3.1 Estimating Ensembles of Model Parameters

Much of the power of the analysis presented here derives from the data assimilation procedure described in section 2.2 and elsewhere. When integrated forward, the estimated model parameter values accurately predict spike timing, subthreshold variation, afterhyperpolarization, spike amplitude and other features within the range of biological trial by trial variability. This even holds true with a basic HH model with only the usual I_{Na} and I_K currents, despite missing many other currents which are present. An exemplar of this data assimilation protocol on the data set is displayed in Figure 1. The model fit and prediction of Figure 1 is among the best, though not by much. The technical difficulty of estimating the many parameters of even a basic HH model is challenging because many of the parameters enter the equations of motion nonlinearily. Although the model fits and predictions such as Figure 1 are often judged subjectively to be quite good, they are not perfect and make mistakes in the prediction.

We do not find that all 3xTg models can be cleanly separated from nonTg. The differences between estimated parameter sets in the two classes may sometimes be subtle or nonexistent. This could reflect the fact that 3xTg and NonTg do not always have strikingly different electrophysiological behavior, or it may be due to present limitations of the model and the fitting procedure. Because

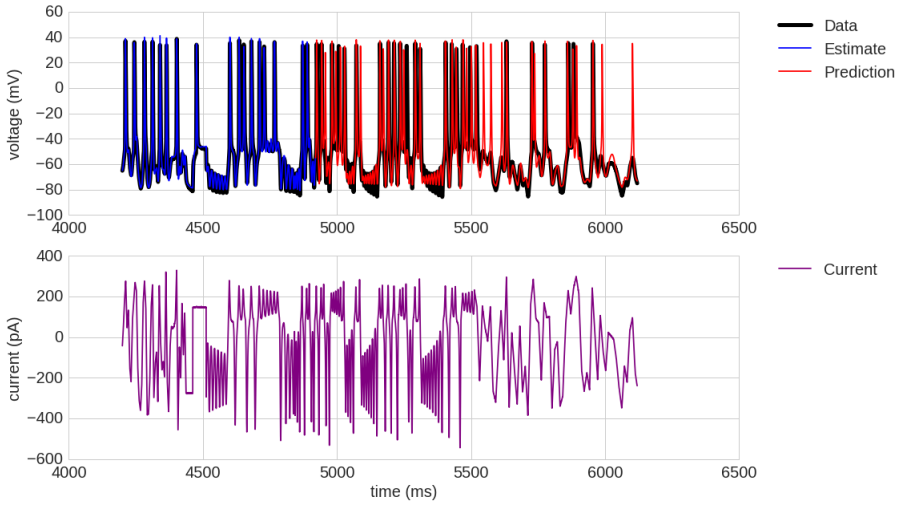

Figure 1: Estimated voltage (blue), stimulating current (purple), data (bold black), and prediction (red), obtained by integrating the estimated model forward in time, shown for a 3xTg neuron. The stimulating current waveform used in the data assimilation procedures is a combination of a pseudo-noisy current and the output of a chaotic model. The pseudo-noisy current was created by uniformly sampling current values about every 20 ms and linearly interpolating in between. The chaotic current waveform is the output from the Lorenz63 model used as a stimulating current.

only 11 neurons were analyzed, some of the differences found may be spurious due to the low sample size. These include some of the passive membrane properties, as discussed in section 3.2.1. Still, in some aspects, clear differences in the neural dynamics do emerge.

3.2 Identifying Differences Between 3xTg and nonTg Neurons

3.2.1 Random Forest Analysis

Figure 2 shows the separation achieved in a subspace including $\tau_{mem} = C_m/g_L$, g_L, and C_m. Among the full set of features tested for differentiating classes of neurons, this and other subspaces including these features are excellent at distinguishing between the two populations as measured by variable importance calculated from the trained random forest classifier. However, the boundary that one can draw between the NonTg and 3xTg strains in subspaces including these features is very complicated. A complicated separating subspace between the two strains may simply be the result of the fact that the number of neurons analyzed is not very large. Therefore, we hesitate to draw any conclusions about whether this separation is biologically significant.

Features Predicting Strain	Var Imp	Centroid Difference
Rheobase (pA/pF)	0.122	-1.648
Threshold Voltage (mV)	0.070	-6.301

Table 1: Features predicting neuron strain (3xTg or NonTg) are calculated using the variable importance from a random forest classifier.

Params Predicting Strain	Var Imp	Centroid Difference
I_{DC} (pA/pF)	0.134	0.954
E_L (mV)	0.117	-1.322
σ_h (mV)	0.096	10.672
θ_m (mV)	0.087	-3.701
σ_{ht} (mV)	0.058	4.535

Table 2: Model parameters predicting neuron strain.

C_m, g_L, and τ_{mem} are therefore excluded from the calculation of variable importances in Table 1. Rheobase, threshold voltage, I_{DC}, and features measuring excitability and properties of I_{Na} and I_K during action potentials are the most important distinguishing characteristics. Rheobase is defined as the lowest value at which a sustained step current first causes an action potential. The voltage at which this occurs is the threshold voltage. $I_{DC} = g_L E_L$ is a DC current which describes passive membrane properties of the neuron.

The time derivative of the ionic currents were calculated at the threshold voltage during an action potential, denoted $\dot{I}_{Na}(V_{thres})$. There are two times at which the voltage passes through the threshold value, one during the upstroke, and one during the downstroke. There was a pattern detected of altered values between the two strains in the time derivaties of I_{Na} and I_K at threshold voltage. However, the magnitudes of I_{Na}, I_K, and their time derivatives were not found to be altered. It is not clear why $\dot{I}_{Na}(V_{thres})$ and $\dot{I}_K(V_{thres})$ are effective predictors of neuron strain, but altered V_{thres} may partly account for this.

I_{DC} is associated with a measure of excitability distinct from, though sometimes related to, reduced threshold voltage or rheobase. In the model, increasing E_L increases I_{DC}, which can counteract repolarizing currents such as I_K during trains of action potentials and reduce depolarizing currents needed to generate an action potential. Larger I_{DC} does not consistently predict decreased threshold voltage and current in the set of estimated models. Instead, I_{DC} may be related to these values in more complicated ways. In some cases, increased I_{DC} is increased as a compensatory mechanism to retain a similar threshold voltage when properties of I_K and I_{Na} are altered. Still, in Table 4, increased I_{DC} does have an overall weak negative correlation with rheobase. A similar explanatory principle may account for why other features effectively predicting the value of a given feature in a regression tree structure show only weak correlations in Tables 3 and 4.

Alterations in the kinetic properties of I_{Na} and I_K in the two strains of

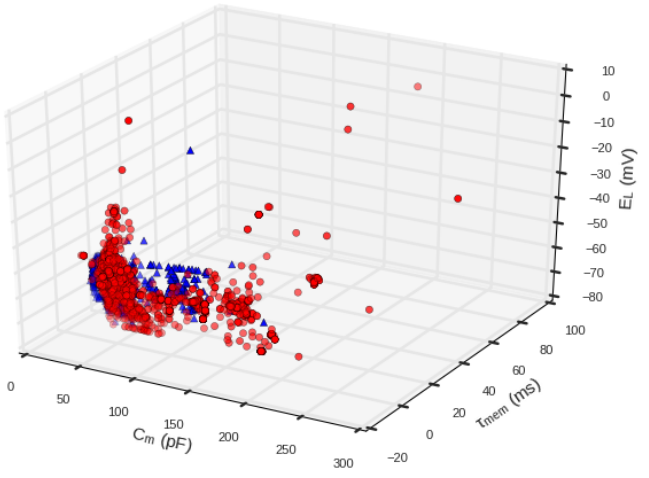

Figure 2: The (C_m, $\tau_{mem} = C_m/g_L$, E_L) subspace gives one of the best separations between the two classes, consistent with the calculated variable importances, but the separation is complex and does not have a clear interpretation. 3xTg estimated values plotted in red, nonTg cells in blue. Other subspaces, such as those of Figures 3 and 4, give separations of 3xTg and nonTg values which are simpler with attendant mechanistic interpretations.

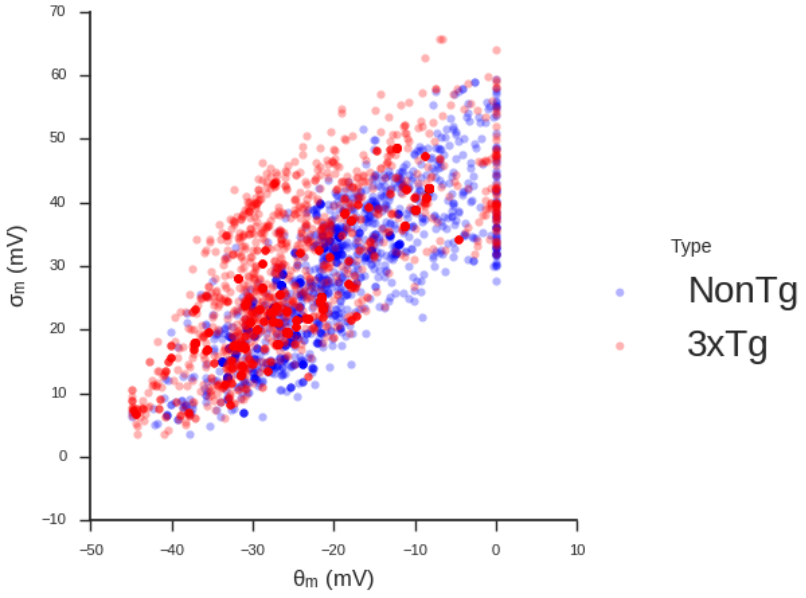

Figure 3: Using the eigenvectors and eigenvalues of the feature correlation matrix, we find that θ_m and σ_m are modestly collinear. In two dimensions the separation between the two classes of neurons becomes stronger than in the case of either of θ_m or σ_m individually.

neurons were also detected. Altered parameters are listed in Table 2. The regression forest models of Tables 3 and 4 show that θ_m, θ_h, and σ_h are important predictors of threshold voltage and rheobase. These are features which are different between neuron strains in the random forest model of Table 1. The two random forest models predicting strain then complement each other, with the regression forest models predicting rheobase and threshold voltage helping to provide a coherent picture of the altered mechanisms underlying these observed differences.

In the (θ_m, σ_m) subspace, shown in Figure 3, a separation between 3xTg and nonTg cells is apparent and provides evidence that altered kinetics in I_{Na} results in a lower threshold voltage in 3xTg. In fact, θ_m and σ_m are found to be modestly collinear from an analysis of eigenvalues and eigenvectors of the feature correlation matrix. Therapeutic remedies could be screened in one way by checking for whether they can shift the value of θ_m and/or σ_m in 3xTg cells into the nonTg regime of Figure 3.

All Params Predicting Threshold Voltage	Var Imp	Correlation
θ_m (mV)	0.208	0.392
τ_{mem} (ms)	0.127	-0.320
σ_h (mV)	0.081	-0.363

Table 3: Feature importances for threshold voltage using only the model parameters as predictors.

All Params Predicting Rheobase	Var Imp	Correlation
θ_h (mV)	0.154	0.183
τ_{mem} (ms)	0.111	-0.283
I_{DC} (pA/pF)	0.098	-0.146
g_{Na} (nS)	0.077	-0.295
θ_m (mV)	0.063	0.224

Table 4: Feature importances for rheobase using only model parameters. I_{DC} is itself a current and τ_{mem} describes the extent to which the membrane smoothes excitatory currents.

3.2.2 Strain Probability Distribution Overlap

We calculated Gaussian kernel density estimates (KDEs) of the probability distributions over three and four dimensional feature subspaces, grouped by strain. Subspaces achieving the best separation were consistent with highly predictive features of the random forest models (Table 5). As the overlap percentages alone do not give sufficient information to determine the nature of the separations, visualizing the feature separations is mandatory. Passive membrane properties tended to give complex separation surfaces (Figure 2), while separations using kinetic properties of ionic current tended to be simpler (Figure 4).

As the dimension of the feature subspaces increases, their number increases factorially, while computational cost of calculating the KDEs grows exponentially. Therefore, it is not feasible to scale this approach up to higher dimensions, and evaluating feature importances using random forest models is preferred.

3D Subspace	Overlap Percentage
(C_m (pF), E_L (mV), τ_{mem} (ms))	0.213
(Rheobase (pA/pF), Threshold Voltage (mV), I_{DC} (pA))	0.368

Table 5: Overlap was calculated between probability density functions for the two strains in three and four dimensional subspaces representing a particular strain. Subspaces achieving the best separation are in accordance with the top ranked random forest variable importance features. The probability distributions are kernel-density estimates using Gaussian kernels. Details about the specific implementation can be found in the scipy documentation. We repeated the calculation for all four dimensional feature subspaces. In four dimensions the subspace (Threshold Voltage (mV), $\dot{I}_{Na}(V_{thres})$ Downstroke (pA/pF/ms), $\dot{I}_{Na}(V_{thres})$ Upstroke (pA/pF/ms), $\dot{I}_K(V_{thres})$ Downstroke (pA/pF/ms)) has the minimal overlap of 3.6%.

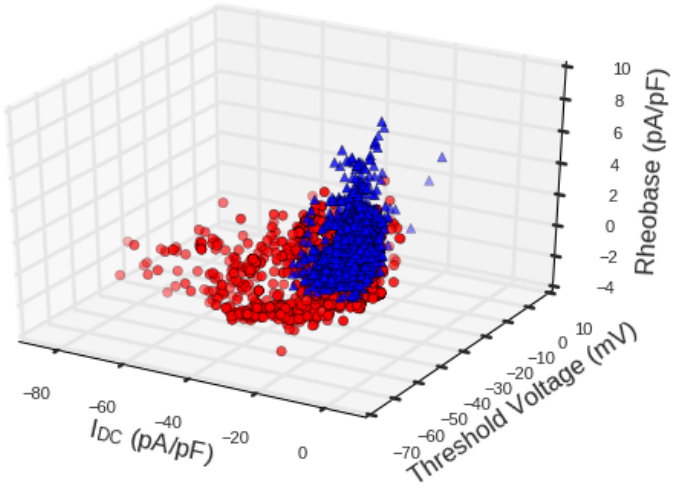

Figure 4: One subspace demonstrating a simple separation with minimal overlap between the neuron strains. The separating features include those associated with neuron excitability and are consistent with features selected by the random forest model.

4 Discussion

Electrophysiological experiments typically carried out to characterize membrane properties are tedious and laborious. The assimilation filter and data mining procedure presented here together constitute a less time consuming and expensive approach. With this approach, it is possible to infer the electrical properties, in detail, across a sizeable population of neurons. This makes it possible to characterize variability and to discover multifaceted differences which might otherwise be lost due to low sample size and averaging.

A present obstacle is the model identifiability problem arising from the numerical difficulty of assimilating data to biophysical models which are too complex. Here we have limited our analysis to detecting alterations in intrinsic excitability of neurons. Consistent with other work bath applying extracellular Aβ to 1 month old WT mice, we have found a hyperpolarized threshold voltage [40, 41] as well as a reduced rheobase in 3xTG mice. Our combined modeling and data mining approach additionally provides possible mechanisms underlying the altered features. We mainly find alterations in the I_{DC} component of the leak current and I_{Na}. Others have found a reduction in I_{Na} [5] or reductions in I_K [31]. In contrast, we primarily see alterations in the gating kinetics of I_{Na}.

We do not find an alteration in spike width. Reductions [40, 41] and broadening [31] in spike width have been found elsewhere. The discrepencies are possibly due to differing mouse models used across studies.

An increased AHP through Ca^{2+}-sensitive K^+ conductances has been noted elsewhere [14, 38]. Our model with only I_{Na} and I_K cannot detect this AHP, as it requires a slower current such as I_{SK} which is sensitive to intracellular Ca^{2+}. Incorporating intracellular Ca^{2+} dynamics will be the goal of future work.

References

[1] Henry Abarbanel. *Predicting the future: completing models of observed complex systems*. Springer, 2013.

[2] Pablo Achard and Erik De Schutter. Complex parameter landscape for a complex neuron model. *PLoS Comput Biol*, 2(7):e94, 2006.

[3] UPINDER S Bhalla and JAMES M Bower. Exploring parameter space in detailed single neuron models: simulations of the mitral and granule cells of the olfactory bulb. *Journal of Neurophysiology*, 69(6):1948–1965, 1993.

[4] Daniela Bianchi, Addolorata Marasco, Alessandro Limongiello, Cristina Marchetti, Helene Marie, Brunello Tirozzi, and Michele Migliore. On the mechanisms underlying the depolarization block in the spiking dynamics of ca1 pyramidal neurons. *Journal of computational neuroscience*, 33(2):207–225, 2012.

[5] Jon T Brown, Jeannie Chin, Steven C Leiser, Menelas N Pangalos, and Andrew D Randall. Altered intrinsic neuronal excitability and reduced

na+ currents in a mouse model of alzheimer's disease. *Neurobiology of aging*, 32(11):2109–e1, 2011.

[6] Marc Aurel Busche, Gerhard Eichhoff, Helmuth Adelsberger, Dorothee Abramowski, Karl-Heinz Wiederhold, Christian Haass, Matthias Staufenbiel, Arthur Konnerth, and Olga Garaschuk. Clusters of hyperactive neurons near amyloid plaques in a mouse model of alzheimer's disease. *Science*, 321(5896):1686–1689, 2008.

[7] Shreaya Chakroborty and Grace E Stutzmann. Calcium channelopathies and alzheimer's disease: Insight into therapeutic success and failures. *European journal of pharmacology*, 739:83–95, 2014.

[8] Johanna L Crimins, Amy Pooler, Manuela Polydoro, Jennifer I Luebke, and Tara L Spires-Jones. The intersection of amyloid beta and tau in glutamatergic synaptic dysfunction and collapse in alzheimer's disease. *Ageing research reviews*, 12(3):757–763, 2013.

[9] Dávid Csercsik, Katalin M Hangos, and Gábor Szederkényi. Identifiability analysis and parameter estimation of a single hodgkin–huxley type voltage dependent ion channel under voltage step measurement conditions. *Neurocomputing*, 77(1):178–188, 2012.

[10] Viviana Culmone and Michele Migliore. Progressive effect of beta amyloid peptides accumulation on ca1 pyramidal neurons: a model study suggesting possible treatments. *Frontiers in computational neuroscience*, 6:52, 2012.

[11] Michele Ferrante, Kim T Blackwell, Michele Migliore, and Giorgio A Ascoli. Computational models of neuronal biophysics and the characterization of potential neuropharmacological targets. *Current medicinal chemistry*, 15(24):2456–2471, 2008.

[12] V Frazzini, S Guarnieri, M Bomba, R Navarra, C Morabito, MA Mariggiò, and SL Sensi. Altered kv2. 1 functioning promotes increased excitability in hippocampal neurons of an alzheimer's disease mouse model. *Cell death & disease*, 7(2):e2100, 2016.

[13] John Hardy. The amyloid hypothesis for alzheimer's disease: a critical reappraisal. *Journal of neurochemistry*, 110(4):1129–1134, 2009.

[14] CC Kaczorowski, E Sametsky, S Shah, R Vassar, and JF Disterhoft. Mechanisms underlying basal and learning-related intrinsic excitability in a mouse model of alzheimer's disease. *Neurobiology of aging*, 32(8):1452–1465, 2011.

[15] Nirag Kadakia, Eve Armstrong, Daniel Breen, Uriel Morone, Arij Daou, Daniel Margoliash, and Henry DI Abarbanel. Nonlinear statistical data assimilation for hvc_ {\ mathrm {RA}} neurons in the avian song system. *Biological Cybernetics*, pages 1–18.

[16] Naomi Keren, Noam Peled, and Alon Korngreen. Constraining compartmental models using multiple voltage recordings and genetic algorithms. *Journal of neurophysiology*, 94(6):3730–3742, 2005.

[17] TL Kerrigan, JT Brown, and AD Randall. Characterization of altered intrinsic excitability in hippocampal ca1 pyramidal cells of the aβ-overproducing pdapp mouse. *Neuropharmacology*, 79:515–524, 2014.

[18] Igor Klyubin, William K Cullen, Neng-Wei Hu, and Michael J Rowan. Alzheimer's disease aβ assemblies mediating rapid disruption of synaptic plasticity and memory. *Molecular brain*, 5(1):25, 2012.

[19] Chris Knowlton, C Daniel Meliza, Daniel Margoliash, and Henry DI Abarbanel. Dynamical estimation of neuron and network properties iii: network analysis using neuron spike times. *Biological cybernetics*, 108(3):261–273, 2014.

[20] Mark Kostuk, Bryan A Toth, C Daniel Meliza, Daniel Margoliash, and Henry DI Abarbanel. Dynamical estimation of neuron and network properties ii: path integral monte carlo methods. *Biological cybernetics*, 106(3):155–167, 2012.

[21] Mark P Mattson, Frank M LaFerla, Sic L Chan, Malcolm A Leissring, P Nickolas Shepel, and Jonathan D Geiger. Calcium signaling in the er: its role in neuronal plasticity and neurodegenerative disorders. *Trends in neurosciences*, 23(5):222–229, 2000.

[22] C Daniel Meliza, Mark Kostuk, Hao Huang, Alain Nogaret, Daniel Margoliash, and Henry DI Abarbanel. Estimating parameters and predicting membrane voltages with conductance-based neuron models. *Biological cybernetics*, 108(4):495–516, 2014.

[23] Durga P Mohapatra, Hiroaki Misonou, Pan Sheng-Jun, Joshua E Held, D James Surmeier, and James S Trimmer. Regulation of intrinsic excitability in hippocampal neurons by activity-dependent modulation of the kv2. 1 potassium channel. *Channels*, 3(1):46–56, 2009.

[24] Tom Morse, Nicholas T Carnevale, Pradeep Mutalik, Michele Migliore, and Gordon M Shepherd. Abnormal excitability of oblique dendrites implicated in early alzheimer's: a computational study. *Frontiers in neural circuits*, 4:16, 2010.

[25] Alain Nogaret, C Daniel Meliza, Daniel Margoliash, and Henry DI Abarbanel. Automatic construction of predictive neuron models through large scale assimilation of electrophysiological data. *Scientific Reports*, 6, 2016.

[26] Jakub Nowacki, Hinke M Osinga, Jon T Brown, Andrew D Randall, and Krasimira Tsaneva-Atanasova. A unified model of ca1/3 pyramidal cells: An investigation into excitability. *Progress in biophysics and molecular biology*, 105(1):34–48, 2011.

[27] Salvatore Oddo, Antonella Caccamo, Masashi Kitazawa, Bertrand P Tseng, and Frank M LaFerla. Amyloid deposition precedes tangle formation in a triple transgenic model of alzheimer's disease. *Neurobiology of aging*, 24(8):1063–1070, 2003.

[28] Salvatore Oddo, Antonella Caccamo, Jason D Shepherd, M Paul Murphy, Todd E Golde, Rakez Kayed, Raju Metherate, Mark P Mattson, Yama Akbari, and Frank M LaFerla. Triple-transgenic model of alzheimer's disease with plaques and tangles: intracellular aβ and synaptic dysfunction. *Neuron*, 39(3):409–421, 2003.

[29] Astrid A Prinz, Cyrus P Billimoria, and Eve Marder. Alternative to hand-tuning conductance-based models: construction and analysis of databases of model neurons. *Journal of neurophysiology*, 90(6):3998–4015, 2003.

[30] Astrid A Prinz, Dirk Bucher, and Eve Marder. Similar network activity from disparate circuit parameters. *Nature neuroscience*, 7(12):1345–1352, 2004.

[31] Federico Scala, Salvatore Fusco, Cristian Ripoli, Roberto Piacentini, Domenica Donatella Li Puma, Matteo Spinelli, Fernanda Laezza, Claudio Grassi, and Marcello D'Ascenzo. Intraneuronal aβ accumulation induces hippocampal neuron hyperexcitability through a-type k+ current inhibition mediated by activation of caspases and gsk-3. *Neurobiology of aging*, 36(2):886–900, 2015.

[32] Dennis J Selkoe. Alzheimer's disease is a synaptic failure. *Science*, 298(5594):789–791, 2002.

[33] Ganesh M Shankar, Shaomin Li, Tapan H Mehta, Amaya Garcia-Munoz, Nina E Shepardson, Imelda Smith, Francesca M Brett, Michael A Farrell, Michael J Rowan, Cynthia A Lemere, et al. Amyloid-β protein dimers isolated directly from alzheimer's brains impair synaptic plasticity and memory. *Nature medicine*, 14(8):837–842, 2008.

[34] Baiyang Sheng, Xinglong Wang, Bo Su, Hyoung-gon Lee, Gemma Casadesus, George Perry, and Xiongwei Zhu. Impaired mitochondrial biogenesis contributes to mitochondrial dysfunction in alzheimer's disease. *Journal of neurochemistry*, 120(3):419–429, 2012.

[35] Cristina Soto-Trevino, Pascale Rabbah, Eve Marder, and Farzan Nadim. Computational model of electrically coupled, intrinsically distinct pacemaker neurons. *Journal of neurophysiology*, 94(1):590–604, 2005.

[36] Grace E Stutzmann. Calcium dysregulation, ip3 signaling, and alzheimer's disease. *The Neuroscientist*, 11(2):110–115, 2005.

[37] Grace E Stutzmann. The pathogenesis of alzheimers disease—is it a lifelong "calciumopathy"? *The Neuroscientist*, 13(5):546–559, 2007.

[38] Grace E Stutzmann, Antonella Caccamo, Frank M LaFerla, and Ian Parker. Dysregulated ip3 signaling in cortical neurons of knock-in mice expressing an alzheimer's-linked mutation in presenilin1 results in exaggerated ca2+ signals and altered membrane excitability. *Journal of Neuroscience*, 24(2):508–513, 2004.

[39] Grace E Stutzmann, Ian Smith, Antonella Caccamo, Salvatore Oddo, Ian Parker, and Frank Laferla. Enhanced ryanodine-mediated calcium release in mutant ps1-expressing alzheimer's mouse models. *Annals of the New York Academy of Sciences*, 1097(1):265–277, 2007.

[40] Francesco Tamagnini, Janet Novelia, Talitha L Kerrigan, Jon T Brown, Krasimira Tsaneva-Atanasova, and Andrew D Randall. Altered intrinsic excitability of hippocampal ca1 pyramidal neurons in aged pdapp mice. *Frontiers in cellular neuroscience*, 9, 2015.

[41] Francesco Tamagnini, Sarah Scullion, Jon T Brown, and Andrew D Randall. Intrinsic excitability changes induced by acute treatment of hippocampal ca1 pyramidal neurons with exogenous amyloid β peptide. *Hippocampus*, 25(7):786–797, 2015.

[42] Anna M Taylor and Roger M Enoka. Optimization of input patterns and neuronal properties to evoke motor neuron synchronization. *Journal of computational neuroscience*, 16(2):139–157, 2004.

[43] Bryan A Toth, Mark Kostuk, C Daniel Meliza, Daniel Margoliash, and Henry DI Abarbanel. Dynamical estimation of neuron and network properties i: variational methods. *Biological cybernetics*, 105(3-4):217–237, 2011.

[44] Andreas Wächter and Lorenz T Biegler. On the implementation of an interior-point filter line-search algorithm for large-scale nonlinear programming. *Mathematical programming*, 106(1):25–57, 2006.

[45] Kenji Yamamoto, Yoshifumi Ueta, Li Wang, Ryo Yamamoto, Naoko Inoue, Kaoru Inokuchi, Atsu Aiba, Hideto Yonekura, and Nobuo Kato. Suppression of a neocortical potassium channel activity by intracellular amyloid-β and its rescue with homer1a. *The Journal of Neuroscience*, 31(31):11100–11109, 2011.

[46] J Ye, N Kadakia, PJ Rozdeba, HDI Abarbanel, and JC Quinn. Improved variational methods in statistical data assimilation. *Nonlinear Processes in Geophysics*, 22(2):205–213, 2015.

[47] Jingxin Ye, Daniel Rey, Nirag Kadakia, Michael Eldridge, Uriel I Morone, Paul Rozdeba, Henry DI Abarbanel, and John C Quinn. Systematic variational method for statistical nonlinear state and parameter estimation. *Physical Review E*, 92(5):052901, 2015.

[48] Hua Zhang, Jie Liu, Suya Sun, Ekaterina Pchitskaya, Elena Popugaeva, and Ilya Bezprozvanny. Calcium signaling, excitability, and synaptic plasticity defects in a mouse model of alzheimer's disease. *Journal of Alzheimer's Disease*, 45(2):561–580, 2015.

[49] Xin Zou, Damien Coyle, KongFatt Wong-Lin, and Liam Maguire. Computational study of hippocampal-septal theta rhythm changes due to beta-amyloid-altered ionic channels. *PLoS One*, 6(6):e21579, 2011.